AIP | Physics of Fluids

Excitation of inertial modes in a closed grid turbulence experiment under rotation

Cyril Lamriben, Pierre-Philippe Cortet, Frédéric Moisy, and Leo R. M. Maas

Citation: Phys. Fluids **23**, 015102 (2011); doi: 10.1063/1.3540660
View online: http://dx.doi.org/10.1063/1.3540660
View Table of Contents: http://pof.aip.org/resource/1/PHFLE6/v23/i1
Published by the American Institute of Physics.

Excitation of inertial modes in a closed grid turbulence experiment under rotation

Cyril Lamriben,[1] Pierre-Philippe Cortet,[1,a)] Frédéric Moisy,[1] and Leo R. M. Maas[2]
[1]*Laboratoire FAST, CNRS UMR 7608, Université Paris-Sud, Université Pierre-et-Marie-Curie, Bât. 502, Campus Universitaire, 91405 Orsay, France*
[2]*Royal Netherlands Institute for Sea Research, P. O. Box 59, 1790 AB Texel, The Netherlands*

(Received 3 September 2010; accepted 29 November 2010; published online 11 January 2011)

We report an experimental study of the decay of grid-generated turbulence in a confined geometry submitted to a global rotation. Turbulence is generated by rapidly towing a grid in a parallelepipedic water tank. The velocity fields of a large number of independent decays are measured in a vertical plane parallel to the rotation axis using a corotating particle image velocimetry system. We first show that, when a "simple" grid is used, a significant amount of the kinetic energy (typically 50%) is stored in a reproducible flow composed of resonant inertial modes. The spatial structure of those inertial modes, extracted by band-pass filtering, is found compatible with the numerical results of L. R. M. Maas [Fluid Dyn. Res. **33**, 373 (2003)]. The possible coupling between these modes and turbulence suggests that turbulence cannot be considered as freely decaying in this configuration. We demonstrate however that these inertial modes may be significantly reduced (down to 15% of the total energy) by adding a set of inner tanks attached to the grid. These results suggest that it is possible to produce an effectively freely decaying rotating turbulence in a confined geometry.
 [doi:10.1063/1.3540660]

I. INTRODUCTION

Translating a grid in a closed volume of fluid is a standard way to generate an approximately homogeneous and isotropic turbulence in order to investigate its temporal decay. Although the level of homogeneity and isotropy of the turbulence generated in this way is not as good as in the more conventional configuration of a fixed grid in an open wind tunnel,[1,2] this closed flow configuration has proved to be very useful when a compact system is needed, and in particular when experiments are performed in a rotating frame.[3–7] Apart from early experiments performed in wind tunnels with a rotating section,[8,9] all rotating grid-generated turbulence experiments since then are based on oscillated or translated grids in closed containers.

Although grid turbulence in open and closed geometries shares similar properties, large scale reproducible flows are more likely produced in the closed configuration.[10] A reproducible flow is defined here as a nonzero ensemble average over several independent realizations of the flow. Such ensemble-averaged flow may actually be triggered from inhomogeneities in the wake of the grid, or from spontaneous symmetry breaking in a perfectly symmetric geometry. In the case of decaying turbulence, although the kinetic energy of the ensemble-averaged flow may be negligible compared to that of turbulence soon after the grid translation, it may persist over large times and possibly influence the final period of decay of turbulence.

In the presence of background rotation, grid-generated turbulence may excite inertial waves. These waves are anisotropic transverse dispersive waves, which propagate through a rotating fluid because of the restoring nature of the Coriolis force.[11,12] Their angular frequency σ lies in the range $[0,2\Omega]$, where Ω is the rotation rate, indicating that these waves can be excited when the characteristic time of the flow is of order of the rotation period, i.e., when the Rossby number is of order unity. The flow excited by a grid translation is, in general, composed of a superposition of (i) a reproducible flow (determined through ensemble averaging) and (ii) a nonreproducible turbulent flow. During the decay of turbulence, both of these two flow components may excite inertial waves after a certain time, when their characteristic timescale decreases down to the order of the rotation period. The excited inertial waves are, respectively, (i) reproducible—and therefore detectable in the ensemble average—and (ii) nonreproducible—detectable in the individual realizations only—and cancel out by phase mixing in the ensemble average since their phase is not coherent between different realizations.

If now the rotating grid turbulence experiments are performed in a closed container, inertial waves may appear in the form of standing inertial modes. Inertial modes are the eigenmodes of a given container geometry, and can be found in general when the walls are either normal or parallel to the rotation axis.[11,13,14] On the other hand, when sloping walls are present, the wave focusing and defocusing induced by the peculiar reflection law of inertial waves[15] preclude the existence of eigenmodes (except in some specific cases such as spheres or ellipsoids), and the concentration of energy along particular beams leads to the so-called wave attractors.[16] However, such attractors are not considered in the following, and we restrict here to the case of eigenmodes. Their resonant frequencies can be derived analytically only in some specific geometries, such as the so-called Kelvin

a)Electronic mail: ppcortet@fast.u-psud.fr.

modes in a cylinder rotating about its symmetry axis.[17] In the case of a parallelepipedic box, the frequencies and the spatial structure of the inertial modes have been characterized in detail by Maas[18] for an inviscid fluid from numerical simulations.

Reproducible inertial modes excited in grid-generated turbulence have been first observed in a parallelepipedic channel with a free surface by Dalziel,[7] who pointed to their potential influence on the decay of the turbulent component of the flow. Inertial oscillations are also clearly visible in the experiments of Morize and Moisy[19] (with a rigid upper surface) and Moisy *et al.*[20] (with a free surface). They have been characterized by Bewley *et al.*[5] in a set of two experiments, in which a grid is rapidly drawn in liquid helium or nitrogen in cylindrical and squared geometries. These authors found good agreement between the measured frequencies and the numerical results of Maas[18] for various aspect ratios. They conclude that translating a grid in a closed rotating container cannot generate freely decaying turbulence because a significant amount of the initial energy may be first stored in the inertial modes, and then gradually released to the turbulence during the decay.

Although none of these experiments investigated the excitation mechanism of inertial modes, it is noteworthy that in all cases those modes were detected in the ensemble-averaged flow, suggesting that they originate from reproducible flow features and not from turbulence. These inertial modes presumably build up from the resonance of phase-coherent inertial waves after multiple reflections over the container walls. As a consequence, if the grid translation is faster than the rotation period (large initial Rossby number), then inertial waves, and hence inertial modes, are expected after a certain time only, when the characteristic time of the resulting flow has decreased down to the order of the rotation period.

The aim of the present paper is to investigate in more details the structure of the inertial modes excited when towing a grid in a rotating square container, and to explore to what extent those modes may be reduced. An experimental setup similar to that of Morize *et al.*[4,19] has been mounted on a new rotating platform, allowing for particle image velocimetry measurements in a vertical plane. We demonstrate that, by attaching a set of inner sidewalls to the grid, the amount of energy stored in the inertial modes may be drastically reduced. A similar configuration has been first shown by Staplehurst *et al.*[6] to reduce significantly the large-scale recirculations in the absence of rotation. We demonstrate here how a configuration inspired from their work strongly reduces the excitation of inertial modes, by an enhanced conversion of the mean flow energy into turbulence.

II. EXPERIMENTAL SETUP

A. Tank and rotating platform

Only the "simple grid" configuration, used in Sec. III, is described here. The modified configuration with additional inner walls is detailed in Sec. IV.

The experimental setup consists in a cubic glass tank, of lateral side $L=60$ cm, filled with 52 cm of water (see Fig. 1),

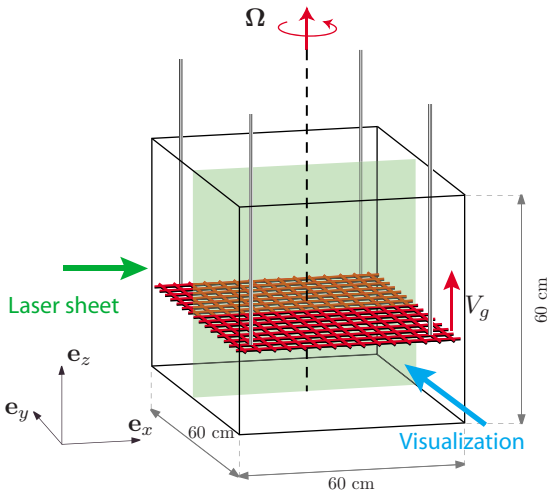

FIG. 1. (Color online) Schematic view of the experimental setup, in the "simple grid" configuration. The $60\times60\times60$ cm^3 tank is filled with 52 cm of water and is rotating at an angular velocity of $\Omega=0.84$ rad s^{-1}. A square grid of 40 mm mesh is towed by four shafts from the bottom to the top at constant velocity $V_g=0.70$ m s^{-1}. PIV measurements in a vertical plane (x,z) are achieved in the rotating frame, based on a laser sheet illuminating the vertical plane (x,z) and a camera aiming normally at it.

and mounted on a precision rotating turntable of 2 m in diameter.[12] The angular velocity Ω of the turntable is set to 0.84 rad s^{-1} (8 rpm), with relative fluctuations $\Delta\Omega/\Omega$ less than 5×10^{-4}. The rotation of the fluid is set long before the experiment (at least 1/2 h) in order for transient spin-up recirculations to be damped and therefore to achieve a solid body rotation. A horizontal cover is placed at a height of $H=49$ cm, defining the upper boundary of the flow.

Turbulence—and inertial modes—is generated by rapidly towing a square grid at a constant velocity $V_g=0.70$ m s^{-1} from the bottom to the top of the tank. During the subsequent decay of turbulence, the grid is kept fixed, at a height of 46 cm, slightly below the cover. The grid consists in 8 mm thick square bars with a mesh size $M=40$ mm, with a solid-to-total area ratio of 0.36. A gap of 3 mm is left between the grid and the sidewalls of the tank. In order to optimize the homogeneity of the flow through the grid, the meshes along the four sides of the grid are actually half meshes. The grid is rigidly attached at its four corners to a servo-controlled brushless motor ensuring the vertical translation of the grid, with acceleration and deceleration phases less than 18% of the total translation time. The Reynolds number based on the grid mesh is $Re_g=V_gM/\nu=28\,000$, and the Rossby number is $Ro_g=V_g/2\Omega M=10.4$, indicating that the flow in the close wake of the grid is fully turbulent and weakly affected by the rotation.

B. Particle image velocimetry (PIV) measurements

Velocity fields in a vertical plane (x,z) are measured using a two-dimensional PIV system. The flow is seeded with 10 μm tracer particles, and illuminated by a corotating vertical laser sheet passing through the center of the tank and generated by a 140 mJ Nd:yttrium aluminum garnet pulsed laser. The entire 60×46 cm^2 flow section is imaged through a transparent side of the tank with a double-buffer high-

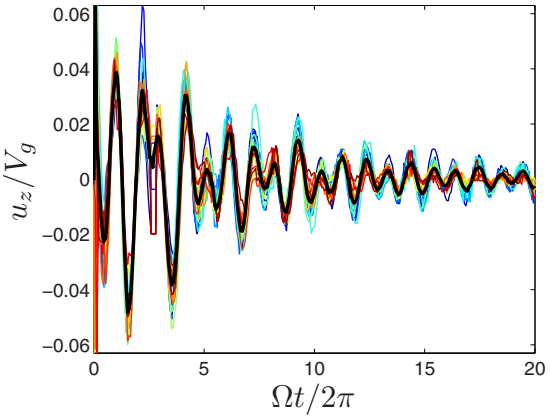

FIG. 2. (Color online) Times series of the vertical velocity $u_z(x_0,z_0,t)$ measured at the center of the flow (x_0=300 mm, z_0=240 mm), for 20 realizations performed at Ω=0.84 rad s^{-1} (in various colors). The black thick line shows the ensemble average of these time series.

resolution 2048×2048 pixels camera, corotating with the tank and aiming normally at the laser sheet. During the decay of turbulence, 428 image pairs are acquired at a sampling rate of 2 Hz. Since the typical flow velocities decrease with time, the delay between the two successive images of a pair is made to gradually increase during the acquisition sequence, from 10 to 68 ms, so that the typical particles displacement remains constant, of order of 5 pixels, during all the decay. PIV computations are then performed over image pairs, on 32×32 pixels interrogation windows with 50% overlap, leading to a spatial resolution of 4.9 mm.

C. Reynolds decomposition

In Fig. 2, we show the time series of the vertical velocity $u_z(x_0,z_0,t)$ at the center of the flow for 20 independent realizations of the decay. The origin t=0 is defined as the time at which the grid reaches the top of the tank. The ensemble average of those realizations is also shown in bold line. This plot clearly illustrates that the flow consists in well-defined oscillations excited by the grid, of characteristic timescale of about one period of rotation, superimposed to nonreproducible turbulent fluctuations. Those oscillations actually correspond to inertial modes, and their amplitude is clearly of the order of the turbulence.

In order to investigate properly the dynamics of the inertial modes and of the turbulence, and the possible coupling between the two, we introduce the standard Reynolds decomposition of the velocity

$$\mathbf{u}(\mathbf{x},t) = \mathbf{U}(\mathbf{x},t) + \mathbf{u}'(\mathbf{x},t). \tag{1}$$

Here $\mathbf{u}(\mathbf{x},t)$ is the total velocity field, $\mathbf{U}(\mathbf{x},t) \equiv \bar{\mathbf{u}}(\mathbf{x},t)$ its ensemble average (i.e., the reproducible component of the flow), and $\mathbf{u}'(\mathbf{x},t)$ its turbulent component. The overbar $\bar{\cdot}$ stands for the ensemble average over several independent realizations of the flow. Note that, although the ensemble average is often approximated by a temporal or a spatial average in most turbulence experiments, the use of true ensemble averages here is critical to separate properly the reproducible nonstationary component of the flow from the turbulence.

The Reynolds decomposition (1) naturally leads to introduce three kinetic energies, characterizing the total, ensemble-average (simply denoted "mean" hereafter), and turbulent flows, respectively, and defined as

$$\begin{aligned} k_{\mathrm{tot}}(t) &= \langle \overline{\mathbf{u}^2}(\mathbf{x},t) \rangle, \\ k_{\mathrm{mean}}(t) &= \langle \mathbf{U}^2(\mathbf{x},t) \rangle, \\ k_{\mathrm{turb}}(t) &= \langle \overline{\mathbf{u}'^2}(\mathbf{x},t) \rangle, \end{aligned} \tag{2}$$

satisfying $k_{\mathrm{tot}}(t)=k_{\mathrm{mean}}(t)+k_{\mathrm{turb}}(t)$. Here the brackets $\langle\cdot\rangle$ denote the spatial average over the whole fluid volume.

In practice, only the two velocity components u_x and u_z can be measured, the measurements being restricted to a vertical plane (x,z) located at midwidth of the tank. The measured kinetic energies must therefore be considered as approximations of the true ones. For a statistically homogeneous and isotropic turbulent component, one would simply have $k_{\mathrm{turb}}^{\mathrm{mes}}=2k_{\mathrm{turb}}/3$. The situation is more complicated for the energy of the mean flow for two reasons: (i) during one period of a given inertial mode, the kinetic energy is basically exchanged between the measured and the nonmeasured velocity components; (ii) the ratio between the energy averaged over the whole tank and the energy averaged over the measurement plane (x,z) only depends on the details of the spatial structure of each mode, which are not known *a priori*. For those reasons, we do not apply here any correcting weight to the velocity components when computing kinetic energies, and we simply define

$$k_{\mathrm{tot}}(t) = \langle \overline{u_x^2}(x,z,t) \rangle_{x,z} + \langle \overline{u_z^2}(x,z,t) \rangle_{x,z} \tag{3}$$

(with $\langle\cdot\rangle_{x,z}$ the average over the vertical plane), and similarly for k_{mean} and k_{turb}. Note that those modified definitions still satisfy the relation $k_{\mathrm{tot}}(t)=k_{\mathrm{mean}}(t)+k_{\mathrm{turb}}(t)$.

III. INERTIAL MODES PRODUCED BY THE SIMPLE GRID CONFIGURATION

A. Kinetic energy decay

In Fig. 3, we present the time evolution of the three kinetic energies (2) computed from 40 decay realizations performed at Ω=0.84 rad s^{-1}. Both the energy of the total and the mean flow show, superimposed to their overall decay, marked oscillations corresponding to the inertial modes. On the other hand, the turbulent energy shows a monotonic decrease, suggesting a good separation between the reproducible and nonreproducible components of the flow. At this point, it is important to note that the kinetic energy of the ensemble-averaged flow $k_{\mathrm{mean}}(t)$ is of the same order than the turbulent one $k_{\mathrm{turb}}(t)$.

The oscillations of $k_{\mathrm{tot}}(t)$ and $k_{\mathrm{mean}}(t)$ are only due to the two-dimension and two-component restriction of the PIV measurements. Indeed, a monotonic decay should be expected for the true energies (2) computed from the three velocity components averaged over the whole fluid volume. We expect therefore that the total and mean kinetic energies are correctly estimated only at the maximum of their oscil-

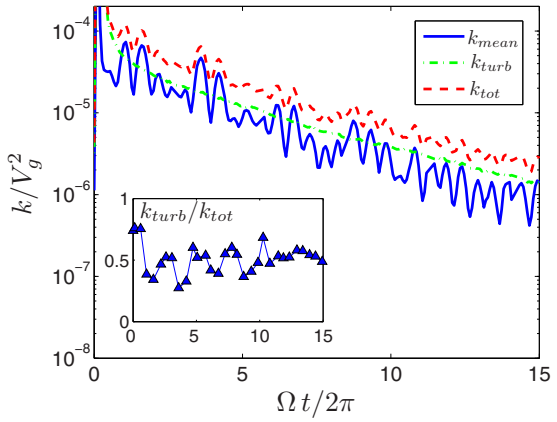

FIG. 3. (Color online) Total (dashed), mean (continuous), and turbulent (dashed-dotted) kinetic energies as a function of the number of tank rotations $\Omega t/2\pi$ from 40 realizations performed at $\Omega=0.84$ rad s^{-1}. Inset: ratio of turbulent to total kinetic energy α (4), measured at times t_n of maximum mean energy.

lations. In order to evaluate the relative amount of turbulent and mean energy in the total flow, we shall therefore consider only the times t_n at which $k_{\text{mean}}(t)$ is maximum, and we introduce the ratio

$$\alpha(t_n)=\frac{k_{\text{turb}}(t_n)}{k_{\text{tot}}(t_n)}. \tag{4}$$

In the inset of Fig. 3, we actually see that turbulence represents only $50\pm10\%$ of the energy in the flow. This quite low ratio indicates that the turbulence produced with this "simple" grid configuration is evenly distributed among the reproducible inertial modes and the "true turbulence." It is therefore questionable to consider this turbulence as freely decaying. Indeed, the possible coupling between the turbulence and the ensemble-averaged flow, which cannot be investigated at this point, may prevent the turbulence to decay freely, as it is continuously fed through energy transfer from the inertial modes.

B. Fourier analysis of the inertial modes

In order to characterize in more details the structure of the flow generated by the grid translation, we perform a temporal Fourier analysis of the ensemble-averaged flow $\mathbf{U}(\mathbf{x},t)\equiv\bar{\mathbf{u}}(\mathbf{x},t)$. Assuming that this ensemble-averaged flow is composed of inertial modes only, $\mathbf{U}(\mathbf{x},t)$ can be written as follows

$$\mathbf{U}(\mathbf{x},t)=\Re\left[\sum_{n,m,s}a_{nms}(t)\mathbf{v}_{nms}(\mathbf{x})e^{i\omega_{nms}t}\right], \tag{5}$$

where $\mathbf{v}_{nms}(\mathbf{x})$ is the (complex) spatial structure of the $[n,m,s]$ mode, ω_{nms} its angular frequency, which lies in the range $[0,2\Omega]$ allowed for inertial waves, and $\Re$ stands for the real part. With notations similar to that of Maas[18] and Bewley *et al.*,[5] we label here the modes using two integer indices, n and m, and a sign, $s=\pm$. The first index n is the normalized vertical wavenumber such that the horizontal (respectively, vertical) velocity component has n (respectively, $n-1$) nodes in the vertical direction. The horizontal structure of a given mode of vertical index n is characterized by the second index m. Larger values of m essentially correspond to finer structures in the horizontal direction, although it is not directly related to the number of nodes as for the vertical index n. Finally, the sign s refers to the symmetry of the mode with respect to the rotation axis: $s=+$ for a symmetric mode and $s=-$ for an antisymmetric mode. The frequencies ω_{nms} are increasing functions of n and, at fixed n and s, decreasing functions of m. In the absence of coupling with other modes or with turbulence, the amplitude of each mode, $a_{nms}(t)$, is expected to be a decreasing function of time because of viscous damping.

The modes present in the ensemble-averaged flow are identified from the temporal Fourier transform of the ensemble-averaged velocity field $\mathbf{U}$ at each position in the (x,z) measurement plane

$$\hat{\mathbf{U}}_\sigma(x,z)=\int_{T_{\min}}^{T_{\max}}\mathbf{U}(x,z,t)e^{-i\sigma t}dt. \tag{6}$$

The bounds $T_{\min}$ and $T_{\max}$ have been chosen equal to 1 and 15 rotation periods, respectively. From this, we define the temporal energy spectrum of the mean (ensemble average) flow, spatially averaged over the (x,z) plane, as

$$E_{\text{mean}}(\sigma)=\frac{1}{2\pi}\langle|\hat{\mathbf{U}}_\sigma(x,z)|^2\rangle_{x,z}. \tag{7}$$

In Fig. 4, the spectrum $E_{\text{mean}}(\sigma)$ clearly shows a series of peaks, whose values are listed in Table I. These peak frequencies are in excellent agreement with some of the numerical eigenfrequencies computed (using the same numerical procedure as in Ref. 18) for our experimental aspect ratio $L/H\simeq1.22$. This shows that the translation of the grid, because of its specific drag profile, selects only a small set of specific inertial modes among the dense spectrum of modes evidenced in Ref. 18. In the next subsection, the spatial structures of the observed modes will be confirmed to match the theoretical structures predicted for the $[n,m,s]$ modes of Table I. Those selected modes are among the lowest order modes $(n=1-3)$, probably because their simpler structure better matches the spatial features of the ensemble-averaged flow at early times, i.e., before it is affected by rotation, and also because higher order modes decay faster by viscous damping.

In order to check whether the inertial modes are present only in the ensemble-averaged flow, we also introduce the temporal Fourier transform of the total, $\hat{\mathbf{u}}_\sigma(x,z)$, and of the turbulent velocity field, $\hat{\mathbf{u}}'_\sigma(x,z)$, similarly to Eq. (6), from which we can define the corresponding energy spectra

$$E_{\text{tot}}(\sigma)=\frac{1}{2\pi}\langle\overline{|\hat{\mathbf{u}}_\sigma|^2}\rangle, \tag{8}$$

$$E_{\text{turb}}(\sigma)=\frac{1}{2\pi}\langle\overline{|\hat{\mathbf{u}}'_\sigma|^2}\rangle. \tag{9}$$

As for the kinetic energies, the energy spectra are additive, $E_{\text{tot}}(\sigma)=E_{\text{mean}}(\sigma)+E_{\text{turb}}(\sigma)$. For a given total spectrum $E_{\text{tot}}(\sigma)$, the two spectra E_{mean} and E_{turb} allow us to distinguish between two kinds of inertial modes: (i) reproducible

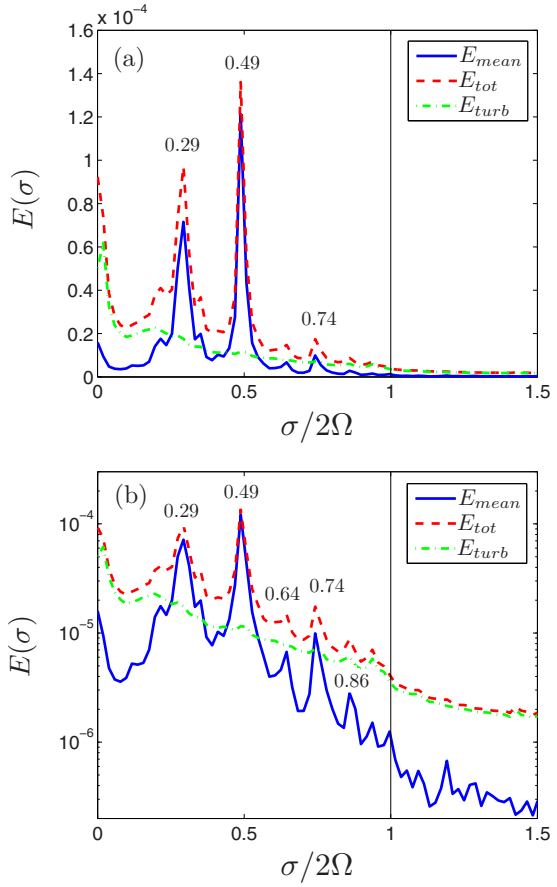

FIG. 4. (Color online) Temporal energy spectrum of the total (dashed), mean (continuous), and turbulent (dashed-dotted) component of the flow as a function of $\sigma/2\Omega$ computed from 40 decay realizations performed at $\Omega=0.84$ rad s^{-1}, with (a) linear and (b) logarithmic y-axis. Inertial modes can develop for angular frequencies $\sigma<2\Omega$. The modes corresponding to the peak frequencies are given in Table I.

(i.e., phase-coherent) modes, characterized by peaks in E_{mean} but not in E_{turb}; (ii) nonreproducible (i.e., random-phase) modes, characterized by peaks in E_{turb} but not in E_{mean}. Interestingly, Fig. 4 shows the complete absence of peaks in the turbulent spectrum $E_{\text{turb}}(\sigma)$, indicating that all the inertial modes present in our system are reproducible and therefore not turbulent. This confirms that inertial modes in this system are more likely excited by reproducible flow features induced by the grid translation.

Finally, it is important to note that more than 97% of the energy of the ensemble-averaged flow lies in the range of angular frequencies $[0,2\Omega]$, confirming that almost all its energy is stored in inertial modes. This result suggests that the ensemble-averaged flow is correctly converged, so that the spectrum of the ensemble-averaged flow is almost not contaminated by the spectrum of residual turbulent fluctuations which span over larger frequencies. On the contrary, we see that there is a significant amount of energy for $\sigma>2\Omega$ in the turbulent spectrum, which actually corresponds to the rapid small scales of usual three-dimensional turbulence which are not directly affected by the rotation.

TABLE I. Numerical values of normalized frequencies $\sigma/2\Omega$ for different modes of order $[n,m,s]$ (where n is the vertical wavenumber, m characterizes the horizontal structure, and s is the symmetry of the mode) compared to the experimental peaks in Fig. 4. The uncertainty of the experimental values is ± 0.01. The numerical values are computed for an aspect ratio identical to the experimental one $L/H=1.22$.

	$\sigma/2\Omega$	
Mode $[n,m,s]$	Num.	Exp.
$[1,4,+]$	0.2992	0.29
$[1,1,+]$	0.4890	0.49
$[1,1,-]$	0.6328	0.64
$[2,1,+]$	0.7429	0.74
$[3,1,+]$	0.8557	0.86

C. Spatial structure of the inertial modes

By performing a band-pass filtering of the ensemble-averaged velocity field at the frequencies of the peaks identified in $E_{\text{mean}}(\sigma)$, it is possible to extract the spatial structure of each inertial mode. Note that this band-pass filtering must take into account the decay of the amplitude $a_{nms}(t)$ of each mode, which is actually reflected in the width of the peaks. Inserting Eq. (5) into Eq. (6) yields

$$\hat{\mathbf{U}}_{\sigma}(\mathbf{x}) = \sum_{n,m,s} \int_{T_{\min}}^{T_{\max}} a_{nms}(t)\mathbf{v}_{nms}(\mathbf{x})e^{i(\omega_{nms}-\sigma)t}dt. \tag{10}$$

If the selected frequency σ coincides with one of the peak frequency ω_{nms} identified in the spectrum, the extracted field is then equal to the spatial structure of the corresponding mode $[n,m,s]$ weighted by its average amplitude

$$\hat{\mathbf{U}}_{\omega_{nms}}(x,z) = \mathbf{v}_{nms}(x,z)\int_{T_{\min}}^{T_{\max}} a_{nms}(t)dt. \tag{11}$$

The resulting spatial structure $\hat{\mathbf{U}}_{\omega_{nms}}(x,z)$ is a complex vector field, whose real and imaginary parts encode the geometric features (amplitude, ellipticity, orientation, and phase) of the elliptic orbit described by the velocity vector at each location during one period. Those orbits can be simply reconstructed by plotting the trace of the real oscillating vector field, $\Re(\hat{\mathbf{U}}_{\omega_{nms}}e^{i\omega_{nms}t})$, for $t\in[0,2\pi/\omega_{nms}]$. The resulting plots for the five dominating inertial modes listed in Table I are shown in Fig. 5. The velocity field, taken for an arbitrary phase of the oscillation, is also illustrated by the vector arrows. The color of the ellipses corresponds to the local ellipticity $-1<\epsilon<1$, where positive ellipticity corresponds to an anticlockwise rotation.

The geometrical features of these fields provide a good qualitative support for the identification of the frequencies given in Table I. In particular, the modes of larger energy are of vertical wavenumber $n=1$ [Figs. 5(a)–5(c)], i.e., they show one cell in the vertical direction. Higher order vertical modes, $n=2$ and $n=3$, are also found, with much weaker energy. The irregular shape of the last mode, $n=3$, is probably due to its very low energy level, and to a possible mixing with other modes of similar frequency. Except for the antisymmetric mode $[1,1,-]$ at $\sigma/2\Omega=0.64$ [Fig. 5(c)], all

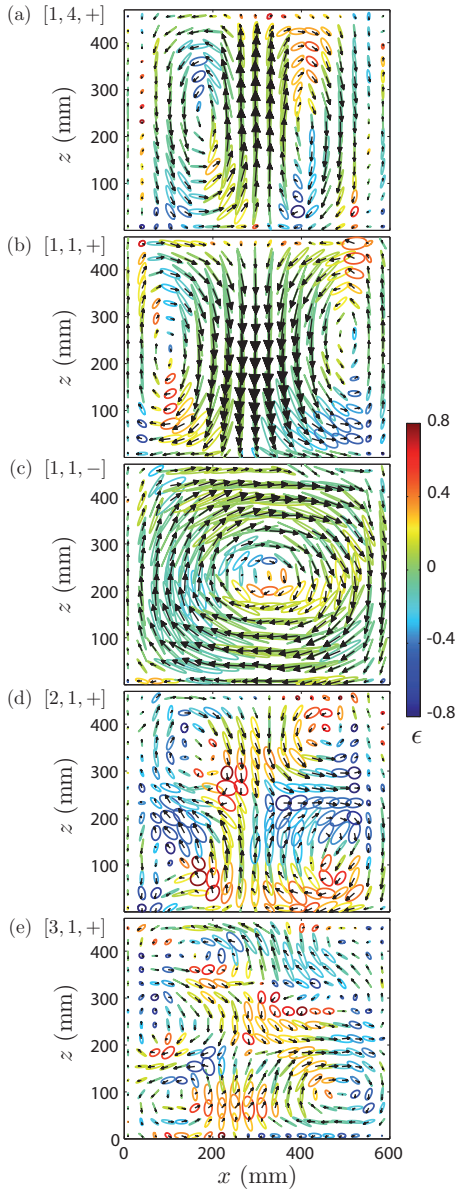

FIG. 5. (Color) Spatial structure of the five dominating inertial modes listed in Table I, extracted by band-pass filtering of the ensemble-averaged fields. The ellipses show the velocity orbit, and the arrows illustrate the velocity field at a given arbitrary phase of the oscillation. The color of the ellipses traces the ellipticity $-1<\epsilon<1$ (see the text for details). (a) [1,4,+]; (b) [1,1,+]; (c) [1,1,−]; (d) [2,1,+]; (e) [3,1,+]. Resolution of the fields has been reduced by a factor 6 for a better visibility.

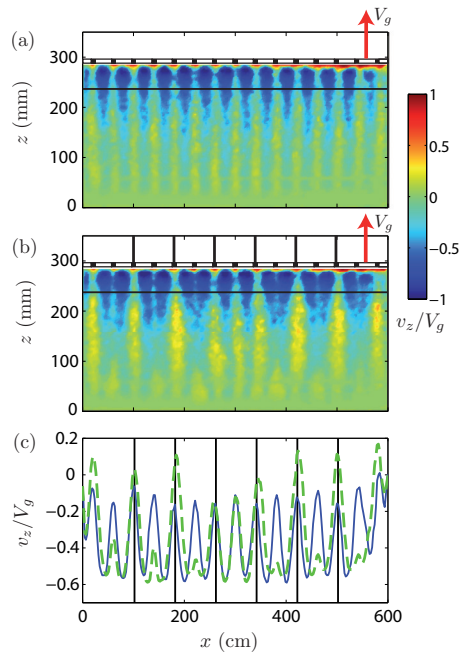

FIG. 6. (Color) Vertical velocity field in the wake of the grid. (a) Simple grid configuration. (b) Modified configuration with the inner walls attached to the grid, represented by the six vertical thick lines. The grid is towed from the bottom, and is at the height $z=290$ mm in these snapshots. (c) Horizontal profile of the vertical velocity, at a distance $\delta z=5$ cm below the grid (indicated by the horizontal lines in a and b). Continuous line: simple grid configuration. Dashed line: modified configuration with inner walls. The vertical black lines show the locations of the vertical inner walls.

the excited modes are symmetric ($s=+$) with respect to the rotation axis. This weak antisymmetric mode is probably excited from a spontaneous symmetry breaking of the flow, or from a slight residual left-right asymmetry of the grid.

The horizontal structure of the modes cannot be inferred from these fields in the vertical plane. However, the visualizations provided in Ref. 18 indicate that, in spite of the square shape of the container, the modes are approximately axisymmetric, at least at a moderate distance from the rotation axis.

The selection of the excited inertial modes among all the possible resonant ones may originate from a residual inhomogeneity of the jet velocities through each mesh of the grid. Such inhomogeneity is not necessarily associated to a defect in the grid, but could arise from the influence of the sidewalls of the tank or from a spontaneous symmetry breaking of the flow. In particular, the spatial structure of the two dominant modes (at $\sigma/2\Omega=0.29$ and 0.49) suggests that larger (or smaller) velocities are produced near the center of the grid, initiating a marked vertical columnar oscillation.

In order to check the possible inhomogeneity of the flow produced by the grid, we have measured the velocity profile just behind the grid during its translation [Fig. 6(a), and the continuous curve in Fig. 6(c)]. Slightly weaker jets are indeed encountered near the borders of the grid, probably originating from the friction with the sidewalls. The resulting rounded average profile could be responsible for the excitation of the dominant symmetric modes.

IV. MODIFIED CONFIGURATION WITH INNER WALLS

A. Comparison with a previous configuration

Although the excitation mechanism of inertial modes in a rotating grid turbulence experiment is interesting in itself, generating such turbulence without those reproducible modes in a confined geometry is also highly desirable. This is motivated by the fact that most theoretical and numerical works on this subject have been performed in purely homogeneous rotating turbulence (in general, made of turbulent inertial waves) without reproducible inertial modes (see, e.g., Sagaut and Cambon[21] and references therein). In this section,

we characterize the flow generated by a modified grid configuration, which turns out to be almost free of inertial modes.

In a similar rotating turbulence experiment, in order to avoid a large scale recirculation flow triggered by the grid translation, Staplehurst *et al.*[6] have designed an original setup in which a parallelepipedic inner tank, consisting in four vertical sidewalls without top and bottom walls, was attached on the upper side of the grid. This inner tank, of 35 cm side, was translated with the grid from the *top to the bottom*, inside the primary 45 cm wide square container filled with water. In this situation, the inner sidewalls are therefore located *downstream* the grid, and once the grid is lowered, the effective flow volume is reduced to the size of the inner tank. With this additional inner tank, these authors actually succeeded to reduce the recirculation flow by a factor 5. However, only the nonrotating case was described, and the possible presence of inertial modes with rotation has not been investigated.

The purpose of the inner tank in the previous downstream configuration was to block the transverse motions in the wake of the grid. Here, in order to force equally distributed jets through the grid, while keeping the full volume for the working fluid, we propose to modify the solution of Staplehurst *et al.*,[6] by adding inner walls located *upstream* the grid. In our configuration, the inner walls are still attached on the upper side of the grid, but the grid here is lifted from the bottom to the top. As a consequence, the working fluid volume in the wake of the grid is the same as in the simple grid configuration, so that direct comparisons of the flow structure can be performed between the two configurations. Several configurations have been tested, with one, two, and three inner tanks. Best results have been obtained with three inner tanks, and only this configuration is described in the following.

B. Modified experimental setup

The new setup is shown in Fig. 7. It consists in three parallelepipedic PVC tanks, of respective height 50, 40, and 40 cm and width 40, 24, and 8 cm. Each tank consists in four vertical sidewalls, without top and bottom walls. The three tanks are fit together coaxially, so that two neighbor sidewalls are separated by two grid meshes, and attached on the upper side of the grid. All other parameters, in particular the grid velocity and Rossby number, are the same as for the simple grid configuration. Since our grid is translated from the bottom to the top, here the inner tanks are *upstream* the grid, so that the decaying flow is not confined inside the smallest tank.

The presence of the inner tanks implies that no horizontal cover could be placed to define the upper boundary of the flow, contrarily to the simple grid configuration. However, we can consider here that an effective upper boundary is approximately defined by the grid itself, locked at a height of 46 cm after its translation. Indeed, we have checked that the simple grid configuration without upper rigid boundary also produces inertial modes, which are as intense as with the rigid boundary. Moreover, here, the inner walls efficiently block the flow in the region between the grid and the free surface.

The velocity field and profiles in this modified configuration are shown in Figs. 6(b) and 6(c), compared to that obtained with the simple grid configuration [Figs. 6(a) and 6(c)]. The main difference is that, now, a stronger upper flow is present in the wakes of those grid bars supporting the sidewalls, whereas the upper flow in the wake of the other grid bars is significantly reduced, and actually even difficult to detect with our PIV resolution. As a consequence, two neighbor jets originating from the same "passage" between two sidewalls tend to gradually merge. At this point, comparing the velocity profiles of the two configurations, with and without the inner tanks, it is not clear whether changes in the energy budget between turbulence and mean flow may arise from the observed differences.

C. Turbulence generated with the grid+inner tanks configuration

The decay of the kinetic energies of the total, mean, and turbulent components of the flow as a function of time, from ensemble averages over 40 decay realizations with the modified configuration, is shown in Fig. 8. In comparison with the simple grid configuration (Fig. 3), the oscillations due to the inertial modes are strongly reduced, both for the mean and the total kinetic energies. We also see that, contrary to the simple grid configuration, the turbulent kinetic energy is now significantly larger than the one of the ensemble-averaged flow. This can be better seen in the inset of Fig. 8, showing that turbulence contains, after a transient of about one tank rotation, approximately $85 \pm 5\%$ of the total kinetic energy, a value much larger than the 50% obtained with the simple grid configuration.

In Fig. 9, we superimpose the temporal energy spectrum of the mean flow obtained with (continuous line) and without (dotted line) the inner tanks. We clearly see that, with the inner tanks, the two dominant peaks (at $\sigma/2\Omega=0.29$ and

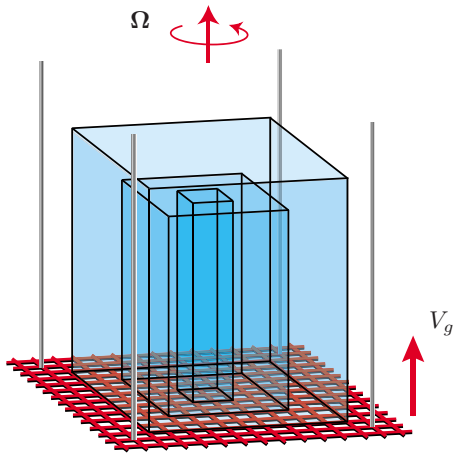

FIG. 7. (Color online) Schematic view of the modified grid configuration (the outer water tank is not shown; see Fig. 1). Three inner tanks are mounted on the grid, and turbulence is generated by raising the set grid +tanks. Each inner tank consists in four vertical sidewalls, without top and bottom walls.

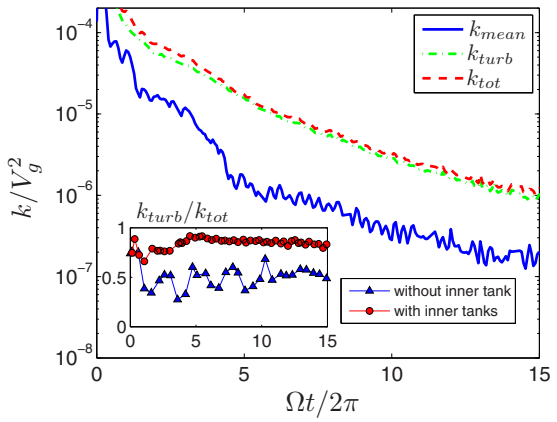

FIG. 8. (Color online) Total (dashed), mean (continuous), and turbulent (dashed-dotted) kinetic energies as a function of reduced time $\Omega t/2\pi$ from 40 decay realizations performed at $\Omega=0.84$ rad s^{-1} with the modified configuration with inner tanks. Inset: ratio of turbulent to total kinetic energy as a function of reduced time $\Omega t/2\pi$ with (points) and without (triangles) inner tanks.

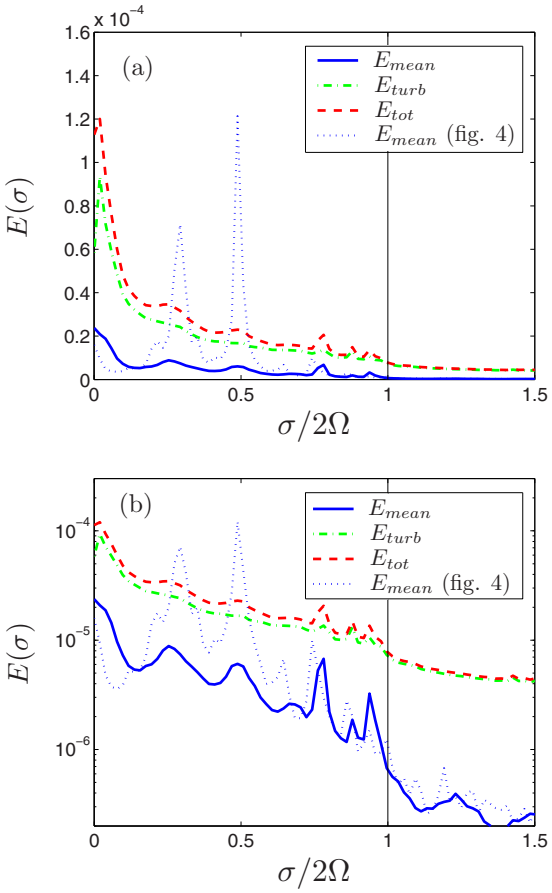

FIG. 9. (Color online) Temporal energy spectrum of the total (dashed), mean (continuous), and turbulent (dashed-dotted) component of the flow as a function of $\sigma/2\Omega$ computed from 40 decay realizations performed at $\Omega=0.84$ rad s^{-1} with inner tanks, with (a) linear and (b) logarithmic y-axis. The dotted line reproduces spectrum of the mean flow for comparison (Fig. 4), obtained with the simple grid configuration.

0.49) have been reduced by more than a factor of 10. The reduction of the other peaks, in particular the $n=2$ mode at $\sigma/2\Omega \simeq 0.74$, is less pronounced. The decrease of the two dominant inertial modes essentially explains the significant drop of the kinetic energy of the mean flow with respect to turbulence shown in Fig. 8. We can also note slight frequency shifts between the two configurations, probably originating from the not perfectly identical boundary conditions at the top of the container, and hence from slightly different effective aspect ratios.

Interestingly, inertial modes are not only absent from the ensemble-averaged flow spectrum, $E_{\text{mean}}(\sigma)$, but also from the turbulent spectrum $E_{\text{turb}}(\sigma)$. This indicates that their disappearance in the modified grid configuration cannot be attributed to a change in the nature of the excited inertial modes, from reproducible to nonreproducible, but to a true disappearance.

The differences in the energy decays and spectra show that the addition of the inner tanks to the grid leads to a much more efficient transfer of the initial mean flow energy into turbulence, bypassing the generation of inertial modes. However, the origin of the changes between the two configurations is not clear. In particular, it is not evident if, and how, the differences in the jet profiles in Fig. 6(c) may explain the preferential energy transfer from the mean flow to the turbulence in the modified configuration. These results illustrate the sensitivity of the inertial modes production to slight changes in the grid geometry, at least for the grid Rossby number considered here, $Ro_g=10.4$.

V. DISCUSSION AND CONCLUSION

In this article, we characterize in details the flow generated when a simple grid is rapidly translated in a rotating and confined volume of fluid. We show that, in addition to a nonreproducible turbulent flow, the grid translation initiates a reproducible ensemble-averaged flow composed of resonant inertial modes, which contain a significant amount of the total kinetic energy. This observation agrees with the recent experiments of Bewley *et al.*[5] in a similar geometry. In addition to quantitative comparisons of the mode frequencies with the numerical predictions of Maas,[18] we also provide here good qualitative comparisons for the spatial structure of these modes.

These results suggest that the turbulent (i.e., the non reproducible) component of the flow generated in this configuration cannot be considered as freely decaying. Indeed, energy transfers between the inertial modes and the turbulence may exist, so that the energy initially stored in the inertial modes may continuously feed the turbulence. However, measuring this transfer would require computing the turbulent Reynolds stress tensor and its coupling with the ensemble-averaged flow. This cannot be performed from the PIV data presented here, which are limited to two velocity components in a single plane.

The ability of a translated grid to generate or not reproducible inertial waves or modes depends on the grid Rossby number, $Ro_g=V_g/2\Omega M$, and also on the geometrical details of the grid configuration, in particular its solidity (ratio of solid to total area). Indeed, for a given grid geometry, a low Rossby number seems more likely to excite inertial modes because the reproducible flow structure in the wake of the grid may directly force inertial waves with a phase coher-

ence. On the other hand, we could speculate that, for much larger Rossby numbers (and assuming that the Reynolds number is very large too), the reproducible wake pattern has more time to loose its coherence before being affected by rotation, so its energy may be more efficiently transferred to turbulence than reproducible inertial waves. Even if inertial waves are later generated from these decaying incoherent motions, their random phase should cancel them out by averaging over independent realizations, so inertial modes should not be found in the ensemble-averaged flow.

In the experiments of Bewley *et al.*,[5] the moderate grid Rossby number Ro_g of 5.5 is found to produce strong inertial oscillations. In the experiments of Staplehurst *et al.*,[6] Ro_g takes even lower values, in the range of 1–3.2, so that significant inertial modes are also expected, although they are not described by these authors. Interestingly, in the present experiment, for a slightly larger grid Rossby number of 10.4, the production of reproducible inertial modes is found to be very sensitive to slight details in the geometry of the grid. Indeed, by adding a set of inner tanks to the grid, we show that it is possible to significantly reduce the production of inertial modes, although the mechanism responsible for this preferred energy transfer toward turbulence instead of modes is not elucidated in the present work. This sensitivity of the flow evidenced for this particular Ro_g is consistent with the results of Morize and Moisy,[19] covering a wide range of Ro_g between 2 and 65, in which a smooth transition around $Ro_g \simeq 10$ was found in the decay law of the turbulent energy, suggesting a change in the energy transfer between inertial modes and turbulence.

A first conclusion from these results is that the standard assumption of statistical homogeneity may not be appropriate to describe decaying rotating turbulence in a closed container. This calls for the development of new experiments and theoretical tools to describe the interaction of turbulence with reproducible inertial modes. However, a second conclusion is that, providing the grid Rossby number and the geometrical features of the grid are carefully selected, achieving a nearly "pure" rotating turbulence, free of reproducible inertial modes, is actually possible in a confined geometry. If these requirements are satisfied, this system may be suitable to explore experimentally the influence of the rotation on freely decaying homogeneous turbulence.

ACKNOWLEDGMENTS

We acknowledge C. Morize and M. Rabaud for discussions about the manuscript, and A. Aubertin, L. Auffray, C. Borget, G.-J. Michon, and R. Pidoux for experimental help. The rotating platform "Gyroflow" was funded by the ANR (Grant No. 06-BLAN-0363-01 "HiSpeedPIV") and the "Triangle de la Physique."

[1] G. Comte-Bellot and S. Corrsin, "The use of a contraction to improve the isotropy of grid-generated turbulence," J. Fluid Mech. **25**, 657 (1966).
[2] S. Mohamed and J. LaRue, "The decay power law in grid-generated turbulence," J. Fluid Mech. **219**, 195 (1990).
[3] A. Ibbetson and D. Tritton, "Experiments on turbulence in a rotating fluid," J. Fluid Mech. **68**, 639 (1975).
[4] C. Morize, F. Moisy, and M. Rabaud, "Decaying grid-generated turbulence in a rotating tank," Phys. Fluids **17**, 095105 (2005).
[5] G. P. Bewley, D. P. Lathrop, L. R. M. Maas, and K. R. Sreenivasan, "Inertial waves in rotating grid turbulence," Phys. Fluids **19**, 071701 (2007).
[6] P. J. Staplehurst, P. A. Davidson, and S. B. Dalziel, "Structure formation in homogeneous freely decaying rotating turbulence," J. Fluid Mech. **598**, 81 (2008).
[7] S. B. Dalziel, "Decay of rotating turbulence: Some particle tracking experiments," Appl. Sci. Res. **49**, 217 (1992).
[8] R. A. Wigeland and H. M. Nagib, "Effects of rotation on decay of turbulence," Bull. Am. Phys. Soc. **23**, 998 (1978).
[9] L. Jacquin, O. Leuchter, C. Cambon, and J. Mathieu, "Homogeneous turbulence in the presence of rotation," J. Fluid Mech. **220**, 1 (1990).
[10] S. P. McKenna and W. R. McGillis, "Observations of flow repeatability and secondary circulation in an oscillating grid-stirred tank," Phys. Fluids **16**, 3499 (2004).
[11] H. Greenspan, *The Theory of Rotating Fluids* (Cambridge University Press, London, 1968).
[12] P.-P. Cortet, C. Lamriben, and F. Moisy, "Viscous spreading of an inertial wave beam in a rotating fluid," Phys. Fluids **22**, 086603 (2010).
[13] D. Fultz, "A note on overstability and the elastoid-inertia oscillations of Kelvin, Solberg, and Bjerknes," J. Meteorol. **16**, 199 (1959).
[14] A. D. McEwan, "Inertial oscillations in a rotating fluid cylinder," J. Fluid Mech. **40**, 603 (1970).
[15] O. M. Phillips, "Energy transfer in rotating fluids by reflection of inertial waves," Phys. Fluids **6**, 513 (1963).
[16] A. M. M. Manders and L. R. M. Maas, "Observations of inertial waves in a rectangular basin with one sloping boundary," J. Fluid Mech. **493**, 59 (2003).
[17] G. K. Batchelor, *An Introduction to Fluid Dynamics* (Cambridge University Press, Cambridge, 1967).
[18] L. R. M. Maas, "On the amphidromic structure of inertial waves in a rectangular parallelepiped," Fluid Dyn. Res. **33**, 373 (2003).
[19] C. Morize and F. Moisy, "Energy decay of rotating turbulence with confinement effects," Phys. Fluids **18**, 065107 (2006).
[20] F. Moisy, C. Morize, M. Rabaud, and J. Sommeria, "Decay laws, anisotropy, and cyclone-anticyclone asymmetry in decaying rotating turbulence," J. Fluid Mech. **666**, 5 (2011).
[21] P. Sagaut and C. Cambon, *Homogeneous Turbulence Dynamics* (Cambridge University Press, Cambridge, 2008).